Test of the Standard Model of Electroweak Interactions by Measuring the Anomalous $ZZ\gamma$ and $Z\gamma\gamma$ Couplings

A Dissertation Presented

by

Gregory Leonid Landsberg

to

The Graduate School

in Partial Fulfillment of the Requirements

for the Degree of

Doctor of Philosophy

in

Physics

State University of New York
at
Stony Brook

December 1994

State University of New York
at Stony Brook

The Graduate School

Gregory Leonid Landsberg

We, the dissertation committee for the above candidate for the Doctor of Philosophy degree, hereby recommend acceptance of the dissertation.

dissertation director
Professor Paul Grannis
Department of Physics

chairman of defense
Professor Michael Marx
Department of Physics

committee member
Professor Peter Koch
Department of Physics

outside member
Professor Ulrich Baur
Department of Physics
SUNY at Buffalo

This dissertation is accepted by the Graduate School.

Graduate School

Abstract of the Dissertation

Test of the Standard Model of Electroweak Interactions by Measuring the Anomalous $ZZ\gamma$ and $Z\gamma\gamma$ Couplings

by

Gregory Leonid Landsberg

Doctor of Philosophy

in

Physics

State University of New York at Stony Brook

1994

A novel test of the gauge sector of the Standard Model (SM) of electroweak interactions — the first measurement of the tri-linear $ZZ\gamma$ and $Z\gamma\gamma$ couplings — was carried out with the DØ detector at the Fermilab Tevatron in $p\bar{p}$ interactions at $\sqrt{s} = 1.8$ TeV. We observed 4 (2) $p\bar{p} \to Z\gamma + X$ events in the dielectron (dimuon) decay channel of the Z, with a total expected background of 0.5 ± 0.1 events, which is in good agreement with SM predictions. The following limits on the anomalous CP-conserving and CP-violating

h_{i0}^V couplings were obtained from fitting the p_T^γ spectrum for a form factor scale of $\Lambda = 500$ GeV (for the case when only one coupling is varied at a time): $|h^Z_{10,30}| < 2.0$, $|h^Z_{20,40}| < 0.5$, $|h^\gamma_{10,30}| < 2.1$, $|h^\gamma_{20,40}| < 0.5$. The results are compared with recent data from the CDF and L3 experiments, as well as with the indirect limits from low energy measurements.

To my Father

Contents

List of Figures

List of Tables

Acknowledgements

Take heart, I said to myself: don't think of Wisdom now; ask the help of Science.

Umberto Eco, "Foucault's Pendulum"

High Energy Physics is an amazing branch of science... Unpredictable, like the fabulous Chicago weather (and like that weather sometimes just pushing you into the lab by simply leaving you no other choice). Being developed around the world by brilliant and devoted people, despite numerous efforts of different governments to terminate their hopes and their future. It is probably the second branch of physics after the space science with a high political impact. Many hate it. Some love it. Which is just the other side of the same coin, since real love is not "for" — it is "despite of." And I must start my acknowledgements with a few nice words about the branch of Science I have chosen.

It is exciting and difficult to work in the field which changes so rapidly. Only 40 years ago the antiproton was discovered at Berkeley. Now, at the Tevatron, we have 50 billion of them in each bunch. About ten years ago the first few W and Z bosons were observed at CERN. It took both the physics and organizing genii of Carlo Rubbia, and many years of hard work of hundreds

of people to build the machine and the detectors capable of fulfilling that goal. Nowadays the W and Z are text-book particles, and I have to use a lint remover to pick up several of them which stuck to my clothes after each visit to the lab.

This Dissertation contains a description of a novel test of the Standard Model of electroweak interactions. In some sense, it is at the leading edge of High Energy Physics today. But it is clear, that in a decade or so the new experiments will improve the results obtained in this first measurement so much, that the two hundred pages of this Thesis will only be of historical interest, and its few remaining copies will comfortably age on dusty shelves of the libraries, with their rusty staples dimly glittering in the dull light turned on by an occasional visitor. And it will be only this preface which still might be up-to-date at that time. Since the things change, but Science itself does not. Because there are, and there always will be people who share their experience and knowledge with the new generations of future scientists, people whom we owe a great debt. And this is why I want this preface to be a bit longer and a bit more broad than a standard acknowledgement section.

First of all I am grateful to my parents who raised me in a scientific spirit. I am the third generation of physicists in my family, and this fact simply left me no other choice than to go into physics. And I do not regret that I did it. I very well remember a phone call which rang in our apartment exactly twenty years ago, one chilly November day of 1974. That morning the discovery of Ψ particle, now known as the J/Ψ, was announced to the world, and somebody called my father, who worked on free quark searches at that time, to tell him

that the fourth quark had just been discovered. There are not too many things which would make my dad to interrupt his morning shower. But this one was apparently among those few. And even though I was only 7 years old at that time, I sort of mentioned to myself, that it must be a really exciting job, which makes you to jump out of the shower and run to the phone! Not that this reminiscence of childhood governed my choice later on, but it must have contributed.

Back to Russia, during my college days and first years of experimental work in the fixed target GAMS experiment, I was lucky to meet many good physicists, and I would like to thank here my first advisor, Yuri Prokoshkin, who taught me a lot about the real work in a modern experiment — both the physics and human aspects.

I would like to thank Mike Marx who introduced me to DØ, a part of which I am proud to be, and who encouraged me to apply to the graduate school of SUNY at Stony Brook.

I owe a great debt to my advisor, Paul Grannis, who first of all acquainted me with the DØ experiment, and helped me a lot during my first days as a graduate student. He always had time for me despite the tremendous workload as the DØ spokesperson. Paul participated in many aspects of this analysis, and several ideas developed here were generated by him. And, most important, during my three years in DØ he always set an example with his broad and deep knowledge of physics and detectors; an example of a complete scientific honesty.

It is a pleasure to express my deep gratitude to Ulrich Baur, who in all senses initiated the analysis described in this Dissertation with a thorough article (written together with E.L. Berger) where many theoretical questions were answered for the first time. He kindly sent me the preprint as soon as it appeared, and this blue book was literally on my table all the time since I started to work on this topic. Ulrich was patient enough to answer in detail tons of my electronic letters with numerous questions about the anomalous couplings which I raised during different stages of the analysis. He also provided us with a fast Monte Carlo program for theoretical calculations, and most of all was a valued friend and advisor for these last two years.

And of course, I am grateful to all members of the DØ family, who built this superior detector, put it into operation, and made this analysis possible at all. I would like to name several people here, who deserve a special "thank you." I owe Sandor Feher, with whom I collaborated on the scintillating fiber detector for tracking chamber calibrations. He introduced me to many DØ folks and helped me in several other aspects. I want to thank my fellow Stony Brook students for being my neighbors in the tight but never dull "cubicles" of the DØ Trailer City. Many people contributed a lot to the analysis described in this Dissertation and kindly did parts of the work for me: Hiro Aihara, Brajesh Choudhary, Mike Kelly, Stefano Lami, and Tony Spadafora. Many more people provided stimulating discussions: Jim Cochran, Marcel Demarteau, Guido Finocciaro, Steve Glenn, Qizhong Li-Demarteau, Meenakshi Narain, Ed Oltman, and Michael Rijssenbeek. I am grateful to Paul Russo and Kim Kwee Ng, computer system managers at Fermilab and Stony Brook, who put a lot of effort into keeping computers working and who helped me to solve numerous software problems. Many thanks also to Jim Cochran, Alain Pluquet, and Scott Snyder who provided me with several detector plots.

I want to thank all the people who read and reread the drafts of this Dissertation and improved it in many aspects by their comments: Ulrich Baur, Jim Cochran, Paul Grannis, Srini Rajagopalan, and Tony Spadafora. Many thanks to Steve Errede of CDF and Fawzi Boudjema from LAPP for a lot of fruitful discussions. I would also like to thank Steve for providing us with the CDF and L3 data.

And last, but not least, I am grateful to many of my friends — beautiful ladies and real gentlemen — who have nothing to do with High Energy Physics, and who simply made my life much more interesting and diverse. I owe to them my numerous trips and a lot of fun in North Carolina and Florida, Atlanta and New York, Boston and Norfolk, Urbana and Binghamton, and of course The Windy City of Chicago. Quoting *"Conquest of Happiness"* by Bertrand Russell,

> *One of the symptoms of approaching nervous breakdown is the belief that one's work is terribly important, and that to take a holiday would bring all kinds of disaster. If I were a medical man, I should prescribe a holiday to any patient who considered his work important...*

And I wish to thank my friends for keep reminding me that there are many important things in life other than my work.

Chapter 1

Introduction

Only for you, children of doctrine and learning, have we written this work. Examine this book, ponder the meaning we have dispersed in various places and gathered again; what we have concealed in one place we have disclosed in another, that it may be understood by your wisdom.

Heinrich Cornelius Agrippa von Nettesheim,

"De occulta philosophia"

The Standard Model of Electroweak Interactions (SM) is one of the most aesthetic theories of modern physics. Developed in the 60's by S.L. Glashow, A. Salam, and S. Weinberg [1], it received its first experimental confirmation in 1973 with the observation of neutral currents in the Gargamelle bubble chamber at the CERN neutrino beam [2]. (Six years later, in 1979, Glashow, Salam and Weinberg won the Nobel Prize for this theory unifying the electromagnetic and the weak interactions.)

A more direct experimental confirmation of the SM was obtained a few years later, in 1983, with the discovery of the intermediate heavy vector bosons

(W and Z) by the UA1 and UA2 Collaborations [3, 4] at the CERN $p\bar{p}$-collider. The significance of this discovery was that the existence of these bosons is a unique and explicit prediction of this theory. Therefore, the search for these particles was a crucial test of the SM.

Numerous experimental tests which have been performed since the discovery of the W and Z bosons have not revealed any deviations from the SM. Currently, the SM based on the special theory of relativity, quantum mechanics, and quantum electrodynamics (QED) has become a cornerstone of our knowledge of Nature.

In the work discussed in the present Dissertation, a novel direct test of the SM has been carried out. We performed a search for anomalous couplings between the Z bosons and photons. This is the first direct experimental test of the SM predictions on the self-interactions between neutral gauge bosons. It has been carried out simultaneously and independently by the DØ and CDF Collaborations at Fermilab and the L3 Collaboration at CERN.

This Dissertation consists of six additional chapters. Chapter 2 (*Theory of the Anomalous Couplings*) gives a brief theoretical overview of the main features of the SM, and a detailed formalism for the description of the $q\bar{q} \to Z\gamma$ process which is sensitive to anomalous couplings between Z's and photons. Various corrections to the tree-level formalism, as well as the sensitivity to the anomalous couplings of indirect low energy experiments, are also discussed in this Chapter. Some models of the anomalous couplings are reviewed. Chapter 3 (*Detector and Monte Carlo*) briefly describes the accelerator and the detector used for the present work, as well as the Monte Carlo program used for detector simulation and precise comparison of the experimental results with the theory. Chapter 4 (*Event Selection*) describes details of the selection of the $p\bar{p} \to Z\gamma$ events in the e^+e^- and $\mu^+\mu^-$ decay channels of the Z, and backgrounds to this process. Possibilities to study this reaction in the $\nu\bar{\nu}\gamma$ channel are also discussed. Chapter 5 (*Limits on the Anomalous Couplings*) contains the main experimental results, which are the limits on the non-SM couplings between Z bosons and photons. Finally, Chapter 6 (*Conclusions*) summarizes the results obtained in the current work and gives some perspectives of future studies of the anomalous couplings with DØ, and with other detectors at existing and projected high-energy colliders. A comparison of the DØ limits with those previously set by direct and indirect low-energy experiments, as well as with the recent direct results from the CDF [5] and preliminary results from L3 [6] Collaborations, is also provided.

Chapter 2

Theory of the Anomalous Couplings

Into every tidy scheme for arranging the pattern of human life, it is necessary to inject a certain dose of anarchism.

Bertrand Russell, "Sceptical Essays"

2.1 Standard Model Formalism

The Standard Model is based on a fundamental $SU(2)_L \times U(1)_Y$ symmetry. There are 4 independent gauge fields which correspond to this symmetry. We will denote a non-Abelian $SU(2)$ field by W^i_μ, $i = 1,\ 2,\ 3$, and an Abelian $U(1)$ field by B_μ. Here and in what follows Greek letters denote Dirac 4-indices.

We further introduce fermions in such a way that they interact both with vector and axial vector currents (in order to explain parity violation in weak decays), and at the same time respect current conservation. This can be achieved by separating left-handed and right-handed fermion fields. The left-handed fields must transform as isospin doublets under $SU(2)$ symmetry, while right-handed fields are isospin singlets. The leptons are entered in the SM as

$$\begin{pmatrix} \nu_\ell \\ \ell^- \end{pmatrix}_L \quad \text{and } \ell_R.$$

There are no right-handed neutrino fields in the SM. Similarly, the quarks are introduced as

$$\begin{pmatrix} u_i \\ d_i' \end{pmatrix}_L, \quad u_{iR}, \text{ and } d_{iR}.$$

Here $\ell = \{e,\ \mu,\ \tau\}$, the index i denotes the three quark families, and d_i' are rotated quark fields: $d_i' = \sum_j V_{ij} d_j$, where V_{ij} is the Cabibbo-Kobayashi-Maskawa mixing matrix [7].

Finally, in order to give masses to the gauge bosons via spontaneous local symmetry breaking (LSB) (Higgs mechanism [8]) we need to introduce an isospin doublet of scalar Higgs fields which preserves only a neutral component after LSB occurs:

$$\varphi = \begin{pmatrix} \varphi^+ \\ \varphi^0 \end{pmatrix} \xrightarrow{LSB} \frac{1}{\sqrt{2}} \begin{pmatrix} 0 \\ v + H \end{pmatrix},$$

where v is the vacuum expectation value (vev) of the Higgs field in the spontaneously broken $SU(2)_L \times U(1)_Y$ symmetry, and H is a new Higgs field with zero vev.

The fermion part of the Lagrangian of the SM after spontaneous symmetry breaking has the following form (see, e.g. [9]):

$$\begin{aligned} \mathcal{L}_{\mathcal{F}} &= \sum_i \bar{\psi}_i \left(i\partial\!\!\!/ - m_i - \frac{g}{2} \frac{m_i}{m_W} H \right) \psi_i \\ &- \frac{g}{2\sqrt{2}} \sum_i \bar{\psi}_i \gamma^\mu (1 - \gamma^5)(T^+ W_\mu^+ + T^- W_\mu^-) \psi_i \\ &- e \sum_i q_i \bar{\psi}_i \gamma^\mu \psi_i A_\mu - \frac{g}{2\cos\theta_W} \sum_i \bar{\psi}_i \gamma^\mu (V^i - A^i \gamma^5) \psi_i Z_\mu . \end{aligned} \tag{2.1}$$

Here $\partial\!\!\!/$ is $\gamma^\mu \partial_\mu$, g and g' are coupling constants for the gauge fields W^i_μ and B_μ; $\theta_W \equiv \tan^{-1}(g'/g)$ is the Weinberg angle; $e = g \sin\theta_W$ is the positron electric charge. The new (rotated) gauge fields are $A \equiv B\cos\theta_W + W^3 \sin\theta_W$ (massless photon field), $W^\pm \equiv (W^1 \mp iW^2)/\sqrt{2}$, and $Z \equiv -B\sin\theta_W + W^3\cos\theta_W$ (charged and neutral heavy weak boson fields). The weak isospin operators are defined as follows: $T_i = \tau_i/2$, where τ_i are Pauli matrices; $T^\pm = T_1 \mp iT_2$; m_W is the mass of the W boson, and m_i are the masses of fermions. Finally, the vector and axial couplings are $V^i \equiv t^i_{3L} - 2q_i \sin^2\theta_W$, $A^i \equiv t^i_{3L}$, where t^i_{3L} is the weak isospin of the i-th fermion ($+1/2$ for ν_ℓ and u_i; $-1/2$ for ℓ and d'_i), and q_i is the charge of ψ_i in units of e.

In short hand notation the last three terms are often put in the first (kinetic) term by replacing $\partial\!\!\!/$ by $\gamma^\mu D_\mu$, where D_μ is a covariant derivative: $D_\mu = \partial_\mu + igW^j_\mu T_j + ig'\frac{1}{2}B_\mu Y$.

The Lagrangian (2.1) contains only the fermion part and does not include cubic and quartic self interactions of W, Z, and γ gauge bosons, as well as cubic and quartic Higgs boson self couplings, and couplings of the Higgs field to the gauge bosons.

The Higgs part of the Lagrangian has the following form:

$$\begin{aligned}
\mathcal{L}_\varphi &= \frac{1}{2}(\partial H)^2 - \frac{1}{2}m_H^2 H^2 \\
&- \frac{1}{8}m_H^2 v^2 \left(-1 + \frac{4H^3}{v^3} + \frac{H^4}{v^4}\right) \\
&+ \frac{1}{4}g^2 W^+_\mu W^{-\mu}(v+H)^2 + \frac{1}{8}\frac{g'^2}{\sin^2\theta_W} Z_\mu Z^\mu (v+H)^2,
\end{aligned}$$

where m_H is the mass of the Higgs particle. It contains kinetic and mass terms for the Higgs scalar (the first two terms), as well as W and Z boson mass terms:

$$m_W^2 W_\mu^+ W^{-\mu} + \frac{1}{2} m_Z^2 Z_\mu Z^\mu,$$

with $m_W = gv/2$, $m_Z = g'v/2\sin\theta_W = m_W/\cos\theta_W$. The second line describes cubic and quartic self interactions of the Higgs field, and the remaining pieces of the last two terms:

$$\left(\frac{1}{4} g^2 W_\mu^+ W^{-\mu} + \frac{1}{8}\frac{g'^2}{\sin^2\theta_W} Z_\mu Z^\mu\right)(H^2 + 2vH)$$

are responsible for WWH, ZZH, $WWHH$, and $ZZHH$ interactions.

Finally, the gauge boson part of the Lagrangian has the following form:

$$\mathcal{L}_W = -\frac{1}{4} W_{i\mu\nu} W_i^{\mu\nu} - \frac{1}{4} B_{\mu\nu} B^{\mu\nu}, \tag{2.2}$$

with

$$\begin{aligned} W_{i\mu\nu} &\equiv \partial_\mu W_{i\nu} - \partial_\nu W_{i\mu} - g f_{ijk} W_{j\mu} W_{k\nu}; \\ B_{\mu\nu} &\equiv \partial_\mu B_\nu - \partial_\nu B_\mu, \end{aligned}$$

where f_{ijk} are the structure constants of the weak isospin group: $[T_i, T_j] = i f_{ijk} T_k$. In the standard representation of the $SU(2)$ group $T_i = \frac{1}{2}\tau_i$, and $f_{ijk} = \epsilon_{ijk}$ (totally antisymmetric tensor). This part of the Lagrangian is responsible for cubic (WWZ, $WW\gamma$) and quartic ($WWWW$, $WWZZ$, $WWZ\gamma$, and $WW\gamma\gamma$) self-interactions of the gauge fields.

There are three free independent parameters which determine the gauge sector of the standard model: g, g', and $v = 2m_W/g = (\sqrt{2}G_F)^{-\frac{1}{2}}$. For low energy electroweak interactions an equivalent set of parameters is normally used: the fine structure constant $\alpha = e^2/(4\pi) = 1/(137.035\,989\,5 \pm 0.000\,006\,1)$ [9], the Fermi coupling constant $G_F = (1.166\,39 \pm 0.000\,02) \cdot 10^{-5}$ GeV^{-2} [9], and the Weinberg angle θ_W. The first two parameters have been measured very precisely using the quantum Hall effect [10] and muon lifetime experiments [11], leaving θ_W as the single parameter to be pinned down. (After the discovery of the W and Z bosons, this last parameter has been precisely measured at LEP and SLC to be $\sin^2\theta_W = 0.2319 \pm 0.0005$ [9].)

In the mass sector of the Lagrangian all masses except that of the Higgs boson and the mass of top quark m_t have been measured[1], so the SM has a very strong predictive power.

Another essential feature of the SM is renormalizability, which was first "guessed" by Weinberg and later proved by t'Hooft [13]. The fact that the SM is renormalizable makes it possible to calculate radiative corrections to the SM in a well defined way. The accuracy of the most precise current experiments (such as measurement of the line shape of the Z resonance at LEP [14]) is high enough to make them sensitive to $\mathcal{O}(\alpha)$ radiative corrections.

2.2 Self-Interactions of Gauge Bosons

An interesting theoretical question which arises in the SM is the self-interaction of gauge fields via trilinear couplings between the carriers, i.e. the vector bosons. (Quartic self-interactions of the gauge fields are beyond

[1]Some evidence for top quark production in $p\bar{p}$ collisions at the Tevatron was recently reported by the CDF Collaboration [12]; the claimed value of the top mass is $m_t = 174 \pm 10^{+13}_{-12}$ GeV$/c^2$.

consideration of this work.)

The W bosons in the SM carry electric charge ($q = \pm e$) and weak isospin charge ($I^W = \pm 1$). The photon and the Z boson are neutral ($q = 0,\ I^W = 0$) and Majorana particles, i.e. they are their own antiparticles.

From the form of the gauge part of the SM Lagrangian (2.2) it is clear that in the SM at tree level the only allowed self-interactions between gauge fields are the interactions between charged and neutral bosons. (These types of interactions for the case of photons are well known and described in QED.) Thus, among all $V_1V_2V_3$ vertices, where V_i is a gauge boson ($V = \{\gamma,\ W^+,\ W^-,\ Z\}$), only the $W^+W^-\gamma$ and W^+W^-Z vertices are non-zero in SM.

The $W^+W^-\gamma$ vertex was first measured directly by the UA2 Collaboration at CERN [15]. The result is consistent with the SM prediction. However the experimental errors are rather large. Both $W^+W^-\gamma$ and W^+W^-Z vertices are currently studied with much higher precision by the CDF and DØ Collaborations at the Fermilab Tevatron, and the results [16, 17] are consistent with the SM. Even more stringent limits on non-SM couplings are expected from future Tevatron experiments and LEP II by the end of this century, and from LHC at the beginning of the next one.

This Thesis is devoted to the study of the trilinear couplings between the neutral gauge bosons, which were never directly tested before. Among the four possible trilinear vertices, ZZZ, $ZZ\gamma$, $Z\gamma\gamma$, and $\gamma\gamma\gamma$, only the first three are allowed by electromagnetic gauge invariance. All of them vanish in SM at tree level. The triple Z vertex, which corresponds to a Z-pair in the final state, is not accessible at present Tevatron energies and luminosities, and can be studied with a reasonable sensitivity only at LEP II operating at center mass energy above $2m_Z$, or at the next generation of hadron colliders. Thus, the current study is restricted to the test of the $ZZ\gamma$ and $Z\gamma\gamma$ vertices, which were first discussed in Ref. [18].

2.3 Probing $ZZ\gamma$ and $Z\gamma\gamma$ Vertices in $q\bar{q}$ Interactions

In this section we discuss in detail the general features of the $ZZ\gamma$ and $Z\gamma\gamma$ vertices in $q\bar{q}$ interactions. In what follows we consider the SM to be valid apart from possible anomalies in these vertices. In particular, we assume that the couplings between quarks or leptons and Z bosons or photons are as predicted by the SM, as has been shown experimentally, e.g. by precise measurement of the leptonic and hadronic widths of the Z at LEP [14].

We will also discuss limits on the anomalous couplings originating from S-matrix unitarity, interference of the trilinear diagram with other types of the diagrams, as well as radiative and QCD corrections to the tree-level diagrams.

2.3.1 $ZZ\gamma$ and $Z\gamma\gamma$ Vertices

Let us consider the general $ZV\gamma$ vertex (see Fig. 2.1), where $V = Z$ or γ. As it was first shown in [19], such a vertex can most generally be described by just four free parameters, h_1^V, ..., h_4^V, assuming only electromagnetic gauge invariance and Lorentz invariance. This can most easily be seen from the following helicity argument. The massless photon of the final state can have only two helicities, -1 or $+1$. The massive Z boson can have in addition helicity 0, which restricts the possible number of different helicity amplitudes for the right side of the diagram in Fig. 2.1 to $2 \times 3 = 6$. However, for the assumption of essentially massless quarks there is no scalar component in the $q\bar{q}V$ vertex, so the virtual boson V is produced purely in the s-channel. Thus, the two combinations which correspond to the opposite helicities of the photon and Z in the final state are excluded, because they require a total helicity of ± 2 for the virtual V, which cannot be accessed via an s-channel exchange of a vector particle. Thus, only four out of six possible helicity amplitudes are allowed, and they generally correspond to four different matrix elements for the trilinear vertex, or four different couplings.

The vertex function for the $ZZ\gamma$ vertex, as derived in [19], has the following form (see Fig. 2.1 for 4-momentum notations):

$$
\begin{aligned}
\Gamma^{Z\gamma Z}_{\alpha\beta\mu} &= \frac{P^2 - q_1^2}{m_Z^2} \left\{ h_1^Z (q_2^\mu g^{\alpha\beta} - q_2^\alpha g^{\mu\beta}) \right. \\
&+ \frac{h_2^Z}{m_Z^2} P^\alpha ((P \cdot q_2) g^{\mu\beta} - q_2^\mu P^\beta) \\
&+ h_3^Z \epsilon^{\mu\alpha\beta\rho} q_{2_\rho} \\
&+ \left. \frac{h_4^Z}{m_Z^2} P^\alpha \epsilon^{\mu\beta\rho\sigma} P_\rho q_{2_\sigma} \right\},
\end{aligned}
\tag{2.3}
$$

where $\epsilon^{\alpha\beta\gamma\rho}$ is a totally antisymmetric tensor, and m_Z is the Z boson mass. Similarly, the $Z\gamma\gamma$ vertex is given by [20]:

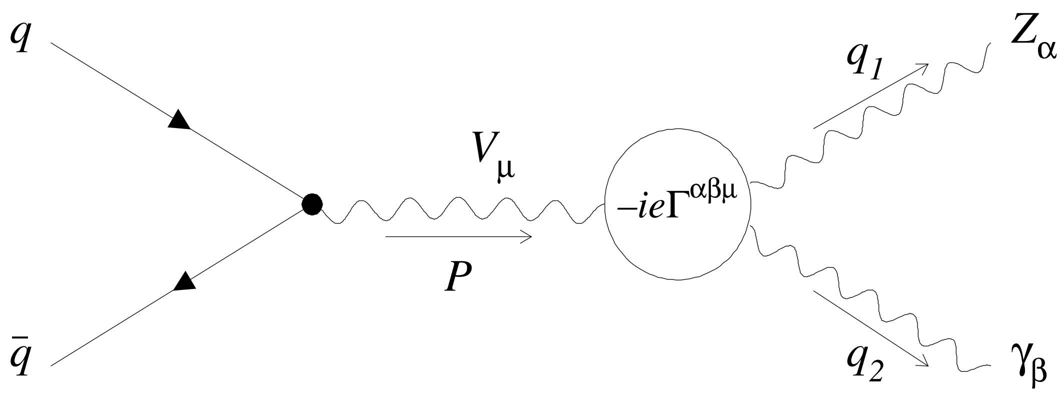

Figure 2.1: Trilinear $ZV\gamma$ vertex in $q\bar{q}$ collisions.

$$\begin{aligned}\Gamma^{Z\gamma\gamma}_{\alpha\beta\mu} &= \frac{P^2}{m_Z^2}\Bigg\{ h_1^\gamma (q_2^\mu g^{\alpha\beta} - q_2^\alpha g^{\mu\beta}) \\ &+ \frac{h_2^\gamma}{m_Z^2} P^\alpha ((P \cdot q_2) g^{\mu\beta} - q_2^\mu P^\beta) \\ &+ h_3^\gamma \epsilon^{\mu\alpha\beta\rho} q_{2\rho} \\ &+ \frac{h_4^\gamma}{m_Z^2} P^\alpha \epsilon^{\mu\beta\rho\sigma} P_\rho q_{2\sigma} \Bigg\}. \end{aligned} \tag{2.4}$$

Terms proportional to P^μ and q_1^α are omitted from (2.3) and (2.4) since they do not contribute to the cross section. The vertex factor is $ie\Gamma^{\alpha\beta\mu}$, which corresponds to the overall coupling constants $g_{ZZ\gamma} = g_{Z\gamma\gamma} = e$. Such a choice does not affect the generality of the expressions (2.3), (2.4); it is simply a definition of the coupling constants h_i^V. In the same fashion the energy scale in the denominator of the overall factor, and in terms proportional to h_2^V, h_4^V is chosen to be the Z mass, because it is a typical mass scale of the trilinear effects. For different mass scales the results can be obtained by a simple scaling [20].

It is important that there is a factor of P^2 in the expression for the $Z\gamma\gamma$ vertex (2.4). As a result, this vertex vanishes when both photons are onshell, which is in agreement with Yang's theorem [21]. This makes it impossible to study the $Z\gamma\gamma$ vertex in two-photon decays of real Z's: one of the photons must be off-shell.

2.3.2 Features of the Coupling Constants

As previously stated (see sec. 2.2), in the SM at tree level, $ZV\gamma$ vertices are zero. Thus, any non-zero couplings h_i^V would mean a violation of the SM, and so the h_i^V are usually referred to as *anomalous couplings.* Some extensions of the SM which predict anomalous couplings will be discussed in sec. 2.5. In this section we are going to discuss general features of the anomalous couplings. Major results discussed here were derived in Refs. [19, 20].

The couplings h_i^V are C-odd dimensionless functions of q_1^2, q_2^2, and P^2. In addition, h_1^V, h_2^V are P-even, and thus violate CP. The other pair: h_3^V, h_4^V, is CP-conserving. As is clear from equations (2.3) and (2.4), h_1^V, h_3^V receive contributions only from operators of dimension ≥ 6, while h_2^V, h_4^V are due to dimension ≥ 8 operators.

To make the anomalous coupling formalism self-consistent, we have to respect the S-matrix unitarity. It was shown in [22] that in order not to violate the unitarity limit, the couplings at high energy should asymptotically approach their SM values, i.e. zero. Therefore, the $ZV\gamma$ couplings have to be energy-dependent, and are thus described by the form factors $h_i^V(q_1^2, q_2^2, P^2)$

which vanish at high q_1^2, q_2^2, or P^2. From the diagram in Fig. 2.1, however, $q_1^2 \approx m_Z^2$, $q_2^2 = 0$, and $P^2 = \hat{s}$. So, only the high $\hat{s}$ behavior should be included in the form factor for the $q\bar{q} \to Z\gamma$ diagrams.

We will use the generalized dipole type of form factors for h_i^V, following Ref. [20]:

$$h_i^V(m_Z^2, 0, \hat{s}) = \frac{h_{i0}^V}{(1 + \hat{s}/\Lambda^2)^n}. \tag{2.5}$$

The constraints on the h_{i0}^V can be derived from the partial wave unitarity of the general $f\bar{f} \to Z\gamma$ process [23, 24]. Assuming that only one coupling is non-zero at a time, the following limits can be derived for $\Lambda \gg m_Z$ [20, 25]:

$$\begin{aligned} |h_{10}^{Z/\gamma}|,\ |h_{30}^{Z/\gamma}| &< \frac{(\frac{2}{3}n)^n}{(\frac{2}{3}n-1)^{n-3/2}} \cdot \frac{0.126/0.151\ \mathrm{TeV}^3}{\Lambda^3}, \\ |h_{20}^{Z/\gamma}|,\ |h_{40}^{Z/\gamma}| &< \frac{(\frac{2}{5}n)^n}{(\frac{2}{5}n-1)^{n-5/2}} \cdot \frac{2.1/2.5 \cdot 10^{-3}\ \mathrm{TeV}^5}{\Lambda^5}. \end{aligned} \tag{2.6}$$

From equations (2.6) it is obvious that unitarity is satisfied only for $n > 3/2$ for $h_{1,3}^V$, and $n > 5/2$ for $h_{2,4}^V$. In what follows we will use $n = 3$ for $h_{1,3}^V$ and $n = 4$ for $h_{2,4}^V$. Such a choice ensures the same asymptotic energy behavior of the $h_{1,3}^V$ and $h_{2,4}^V$ couplings. The dependence of the results on the choice of n is discussed in [20].

Both the unitarity limits and the strength of the couplings depend strongly on the scale parameter Λ. Together with the denominator power n, Λ is a parameter of the model. As long as the choice of n is fixed, the scale Λ is the only free parameter. The actual value of Λ is not predicted by the theory. The physical meaning of this parameter is a "compositeness scale", or scale for new physical phenomena. It is reasonable to expect Λ to be at least of the order of a few hundred GeV. If Λ is too small (say, of the order of m_Z), one would expect the real Z boson to have properties different from what the SM predicts, but there is no evidence for such a difference [14]. Very large values of Λ, on the other hand, will effectively suppress any effects of anomalous couplings due to unitarity limits up to very high energies, which is also unnatural. We will discuss the dependence of the results on the value of Λ scale in Chapter 5.

The anomalous couplings h_i^V are related to the dipole and quadrupole transition moments of the Z boson. Unlike the $WW\gamma$ case, where the anomalous couplings contribute to the above moments of the real particle (i.e. W [26]), $Z\gamma$ couplings do not affect the magnetic or electric moments of the Z boson itself, since the Z is a Majorana particle and thus all its moments are equal to 0 due to the CPT-theorem [27]. The CP-even combinations of h_3^V, h_4^V correspond to the electric dipole and magnetic quadrupole transition moments of the $ZV\gamma$ vertex; the CP-odd combinations of h_2^V, h_4^V correspond to magnetic dipole and electric quadrupole moments. The actual relation between the couplings and moments is rather complicated and depends both on the center of mass (CM) energy ($\sqrt{\hat{s}}$) and on the momentum of the final state photon [28] (unlike the $WW\gamma$ case).

2.3.3 Probing the $ZZ\gamma/Z\gamma\gamma$ Vertices at the Tevatron

Final State Signature and Feynman Diagrams

The formalism of the previous section allows one to calculate the matrix elements for the vertex in Fig. 2.1. This vertex corresponds to a Z boson and a photon on the right-hand side of the reaction. However, experimentally the presence of a Z boson is inferred only by detecting its decay products.

The hadronic modes of Z decay are contaminated with a large QCD multijet background, so at present it is possible to select Z-events only in the leptonic decay modes. Furthermore, it is a rather challenging experimental task to detect the $Z \to \tau^+\tau^-$ decay channel in hadronic collisions, so we will consider only $Z \to e^+e^-$, $Z \to \mu^+\mu^-$, and $Z \to \nu\bar{\nu}$ decay modes. Thus, the final state signature for probing the $ZV\gamma$ vertices is $\ell\bar{\ell}\gamma$, where $\ell = e,\ \mu,$ or ν.

However, the trilinear vertex is not the only one contributing to this final state. The whole set of tree level Feynman diagrams for the processes which produce a lepton pair and a photon in the final state are shown in Fig. 2.2. There are three types of reactions which contribute to the $\ell\bar{\ell}\gamma$ final state. Diagrams a) and b) represent the so-called initial state radiation, when the hard photon is emitted via *bremsstrahlung* of an incoming antiparton (a) or parton (b). Diagram c) corresponds to the already discussed trilinear coupling (or self-interaction) between gauge bosons, and it vanishes in the SM (see sec. 2.2). The only possible combinations of gauge bosons for the anomalous diagram (c) are $ZZ\gamma$ and $Z\gamma\gamma$, since the $\gamma\gamma\gamma$ vertex is prohibited (see sec. 2.2). Finally, the diagrams d) and e) describe radiative decay (or final state radiation), when the photon is emitted by one of the final state leptons, produced mainly in the decays of on-shell Z's. In what follows, we will refer to the diagrams of these three types as to *production* (a-b), *trilinear* (c), or *decay* (d-e) diagrams. It is important that for the neutrino decay channel of

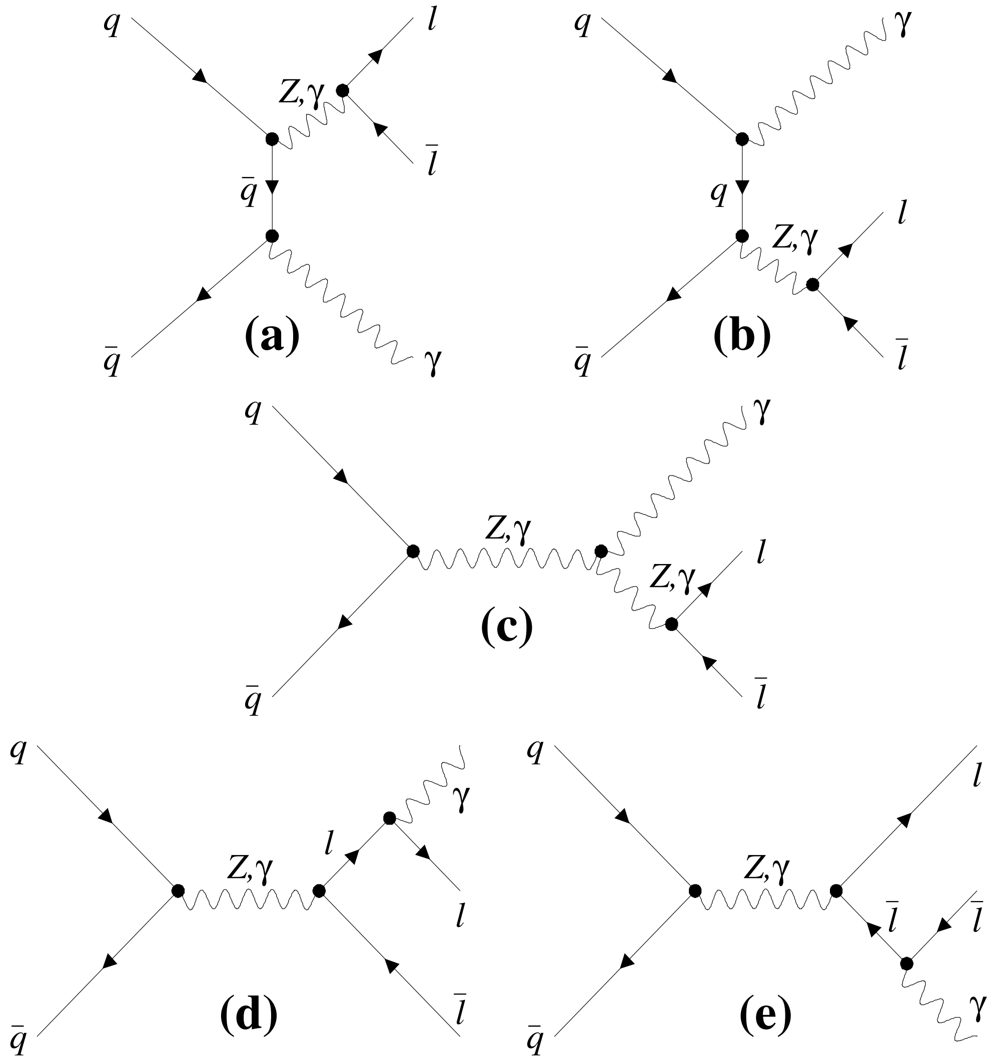

Figure 2.2: Tree level Feynman diagrams for the $q\bar{q} \to \ell\bar{\ell}\gamma$ processes: (a,b) initial state radiation, (c) trilinear coupling, and (d,e) radiative decay.

the Z ($\ell = \{\nu_e,\ \nu_\mu,\ \nu_\tau\}$) the decay diagrams vanish as well, because neutrinos do not interact with photons.

Theoretical calculations of the SM and anomalous cross sections for the whole set of processes pictured in Fig. 2.2 were done by U. Baur and E.L. Berger who kindly provided us with a Monte Carlo generator [20] suitable for obtaining various differential cross sections for the $p\bar{p} \rightarrow \ell^+\ell^-\gamma + X$ and $p\bar{p} \rightarrow \nu\bar{\nu}\gamma + X$ reactions, where X denotes associated QCD jets and soft particles.[2] These calculations take into account finite Z-width effects, interference effects between the diagrams in Fig. 2.2, and a simple detector simulation. We further modified the code and incorporated a more sophisticated and realistic simulation of the DØ detector to enable a more precise comparison between the data and theoretical predictions (see sec. 3.7). However, all numerical results of the current (theoretical) section are obtained with the detector simulation switched off.

The main result of these calculations is that the cross section of the $p\bar{p} \rightarrow Z\gamma$ reaction for the anomalous coupling case ($h^V_{i0} \neq 0$) is *larger* than for the SM case. This means that the diagram in Fig. 2.2 (c) interferes *constructively* with the rest of the diagrams, which gives a very favorable experimental signature for the anomalous couplings: an excess of $\ell\bar{\ell}\gamma$ or $\gamma \not{E}_T$ events.

The cross section of $\ell\bar{\ell}\gamma$ production can be expressed as a bilinear form of the couplings h^V_{i0} with a minimum located very close to the SM values (h^V_{i0} = 0). Thus, it is possible to set limits on the anomalous couplings from a simple counting experiment. There are, however, more advanced and sensitive methods of obtaining these limits, and they will be discussed later in this section and in Chapter 5.

---

[2]In what follows we will omit the X term in the reaction notations, always assuming the inclusive $Z\gamma$ production.

$p\overline{p} \to \ell^+\ell^-\gamma$

The expression for the cross section for

$$p\bar{p} \to \ell^+\ell^-\gamma \tag{2.7}$$

exhibits several different divergences [20]. One is a *collinear divergence* which occurs when the photon is emitted parallel to one of the leptons. Another one is an *infrared divergence* which occurs when the photon has vanishing energy. However, a comparison with a real experiment does not suffer from these theoretical divergences in the Lagrangian for two reasons: (i) it is impossible to detect a photon below a certain energy threshold, and (ii) in order to distinguish between the photon and a lepton, one needs a sufficient spatial separation between these two objects in the detector.

Thus, any real experiment measures the cross section for (2.7) only in a fraction of the total available phase space. It is natural to perform theoretical calculations only for such restricted kinematics. In order to study the signatures for anomalous couplings, we will impose a set of basic cuts, typical for a general-purpose detector working at high energy hadron colliders (such as the DØ or CDF detector). The actual cuts used for event selection (see Chapter 4) are somewhat different from these basic cuts, but the qualitative behavior of the various kinematical distributions we are going to study remains the same. At this point we do not introduce any corrections for momentum smearing and do not consider the detection efficiencies, except for taking into account the finite acceptance of the detector for leptons and photons. The results in this section are calculated for the Tevatron energy ($\sqrt{s}$ = 1.8 TeV) and correspond to a single lepton channel of Z-decay (e.g. e^+e^-). The MRSD$-'$ [29] set of structure functions is used in the simulation (see sec. 3.7 for the discussion of the structure function dependence of the cross section). The effects of next to leading order logarithmic (NLL) QCD corrections are simulated via a scaling factor $k = 1 + \frac{8\pi}{9}\alpha_s \approx 1.34$ (see sec. 2.3.4). The anomalous coupling contribution is calculated for a form factor scale of $\Lambda = 500$ GeV.

The basic set of cuts for the $\ell^+\ell^-\gamma$ production (2.7) is defined as follows:

$$\begin{gathered} p_T^{\ell^\pm} > 15 \text{ GeV}/c, \quad p_T^\gamma > 10 \text{ GeV}/c; \\ |\eta_{\ell^\pm}| < 3.0, \quad |\eta_\gamma| < 3.0; \\ \Delta R_{\ell^\pm\gamma} \equiv \sqrt{(\Delta\phi_{\ell^\pm\gamma})^2 + (\Delta\eta_{\ell^\pm\gamma})^2} > 0.7. \end{gathered} \tag{2.8}$$

Here p_T is the transverse momentum ($p_T \equiv \sqrt{p_x^2 + p_y^2}$ in the lab frame with z along the beam direction); η is the pseudorapidity of the particle: ($\eta \equiv \tanh^{-1}(\cos\theta)$; θ and ϕ are polar and azimuthal angles of the particle momentum in the lab frame, see sec. 3.2.1). In what follows we will refer to ΔR as to the *separation* (in η, ϕ space).

The theoretical cross section of the reaction (2.7) within this set of cuts per one lepton channel is $\sigma(SM) = 2.06$ pb. We will compare the SM and anomalous cases for two different couplings: $h_{30}^Z = 2.5$, and $h_{40}^Z = 0.5$ (varying only one coupling at a time). The theoretical cross section for the anomalous case is somewhat higher: $\sigma(h_{30}^Z = 2.5) = 2.85$ pb, $\sigma(h_{40}^Z = 0.5) = 2.49$ pb. The effect of the anomalous CP-violating h_{10}^Z/h_{20}^Z couplings is very similar (both qualitatively and quantitatively) to that of h_{30}^Z/h_{40}^Z. The contribution of the h_{i0}^γ couplings is a few per cent less than that of the h_{i0}^Z couplings of

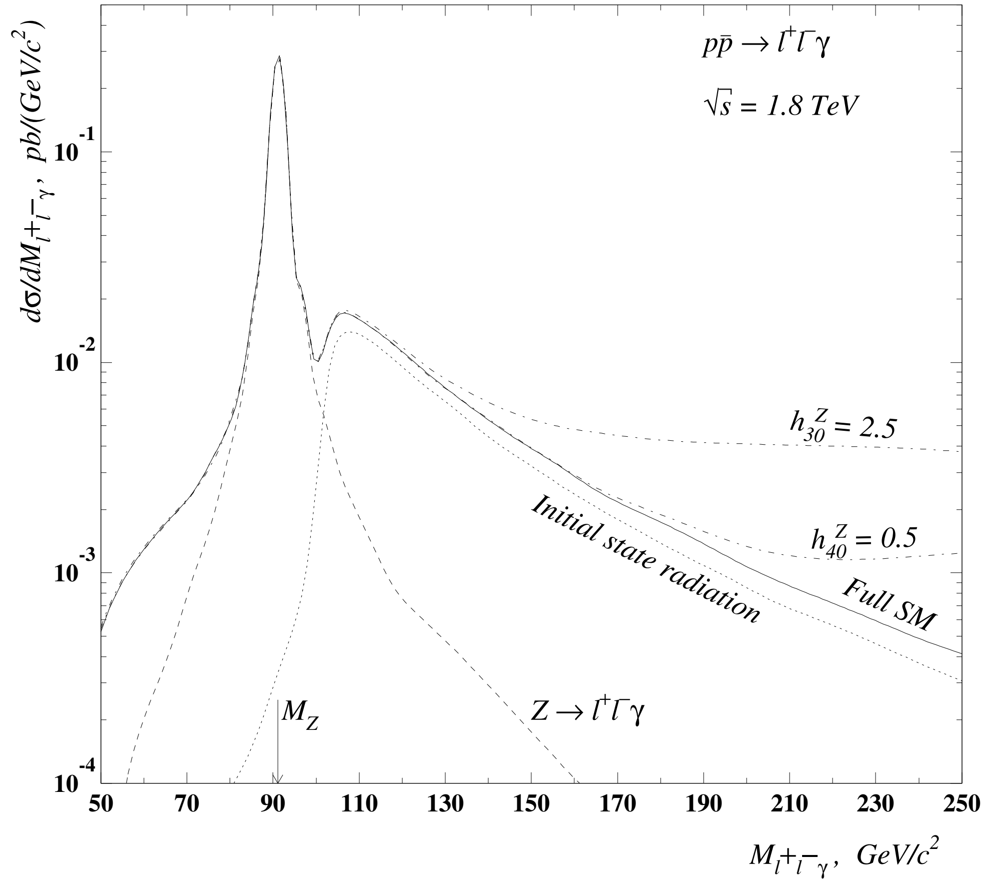

Figure 2.3: Invariant mass of the $\ell^+\ell^-\gamma$ system produced in the reaction (2.7) for different processes contributing to the $\ell^+\ell^-\gamma$ final state. For notations see text.

equal strength. This is true for all plots in this section, so this fact will not be emphasized further, and we will discuss only the signature of the h^Z_{30} and h^Z_{40} couplings.

The following five figures show different kinematical distributions for the final state particles in the reaction (2.7). The invariant mass distribution of the $\ell^+\ell^-\gamma$-system produced in (2.7) is shown in Fig. 2.3. The solid line corresponds to the full SM case. The dashed line shows the part of the SM cross section from the decay diagrams only (see Fig. 2.2 (d, e)), with a real Z produced in the s-channel. As one would expect, a clear Z-peak is seen in the three-body mass spectrum for the decay process. The contribution of the off-shell photon exchange in these diagrams (Drell-Yan production of $\ell^+\ell^-$ pair) is important only at masses below Z-peak and at high masses. It accounts for the difference between solid and dashed (dotted) lines at the lower (upper) edge of the plot. The dotted line represents the contribution of the production diagrams (see Fig. 2.2 (a,b)), or the initial state radiation. It is concentrated at masses above the Z mass, and clearly separated from the decay diagram contribution. At invariant masses $m_{\ell^+\ell^-\gamma} > 100$ GeV/c^2 the production diagrams dominate in the cross section. The sharp dip just above Z mass is due to the $p_T^\gamma > 10$ GeV/c cut. Finally, dash-dotted lines show the anomalous cross sections for the case of $h_{30}^Z = 2.5$ (top) and $h_{40}^Z = 0.5$ (bottom). The notations in the following figures of this section are the same as in Fig. 2.3.

It is important to point out that the effects of anomalous couplings are significant only for high masses of the $\ell^+\ell^-\gamma$ system, or at high $\hat{s}$. This is the reason why one needs a high energy collider to study anomalous trilinear couplings. Note that the effects of h_{30}^Z coupling become noticeable at smaller values of $\hat{s}$ than those of h_{40}^Z, which is a direct consequence of different powers of $\sqrt{\hat{s}}/m_Z$ for h_3^Z and h_4^Z in the vertex function (2.3). At very high energies ($\sqrt{\hat{s}} \gg \Lambda$), however, the asymptotic behaviors of these two couplings become the same due to the appropriate choice of the denominator power in the form factors (2.5) (see sec. 2.3.2).

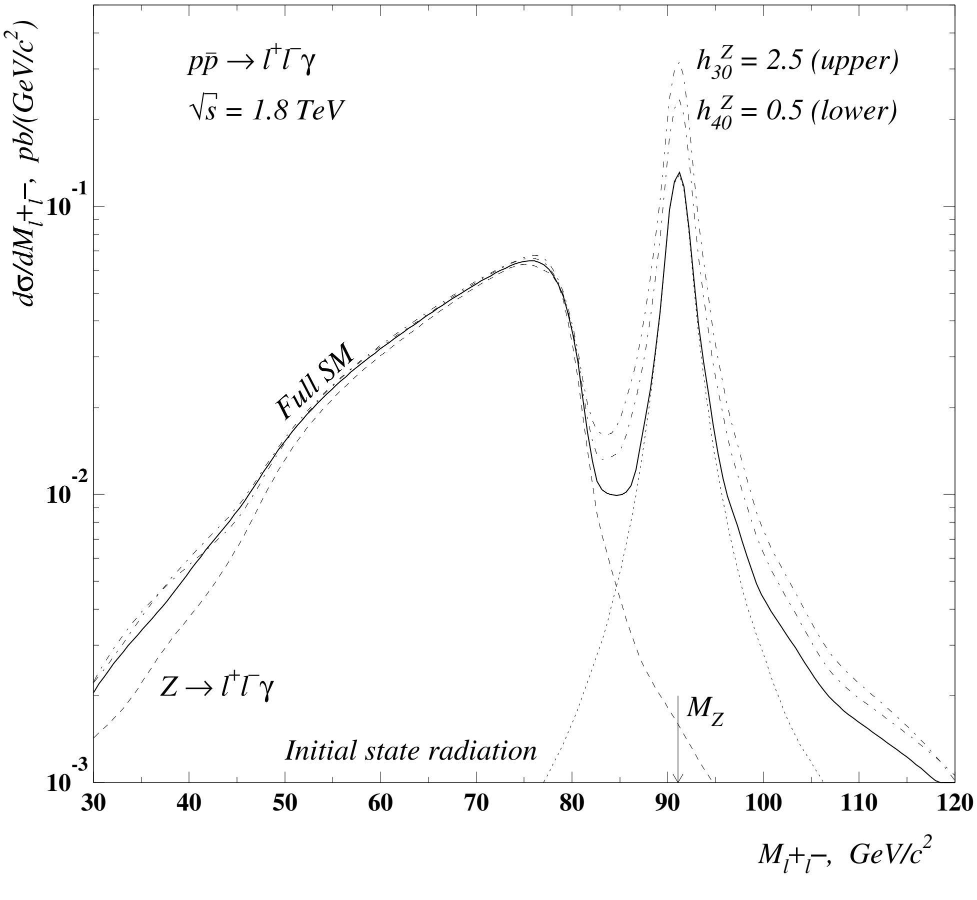

Figure 2.4: Invariant mass of the $\ell^+\ell^-$ system produced in the reaction (2.7) for different processes contributing to the $\ell^+\ell^-\gamma$ final state. For notations see text.

The invariant mass spectrum of the $\ell^+\ell^-$ pair is shown in Fig. 2.4. Here the initial state radiation and anomalous coupling effects are concentrated in the Z-peak region, whereas the decay diagrams populate the lower part of the spectrum. Again, decay and production diagram contributions are clearly separated. The strong dip at ≈ 80 GeV$/c^2$ is due to the finite p_T^γ cut, similar to that in the previous plot.

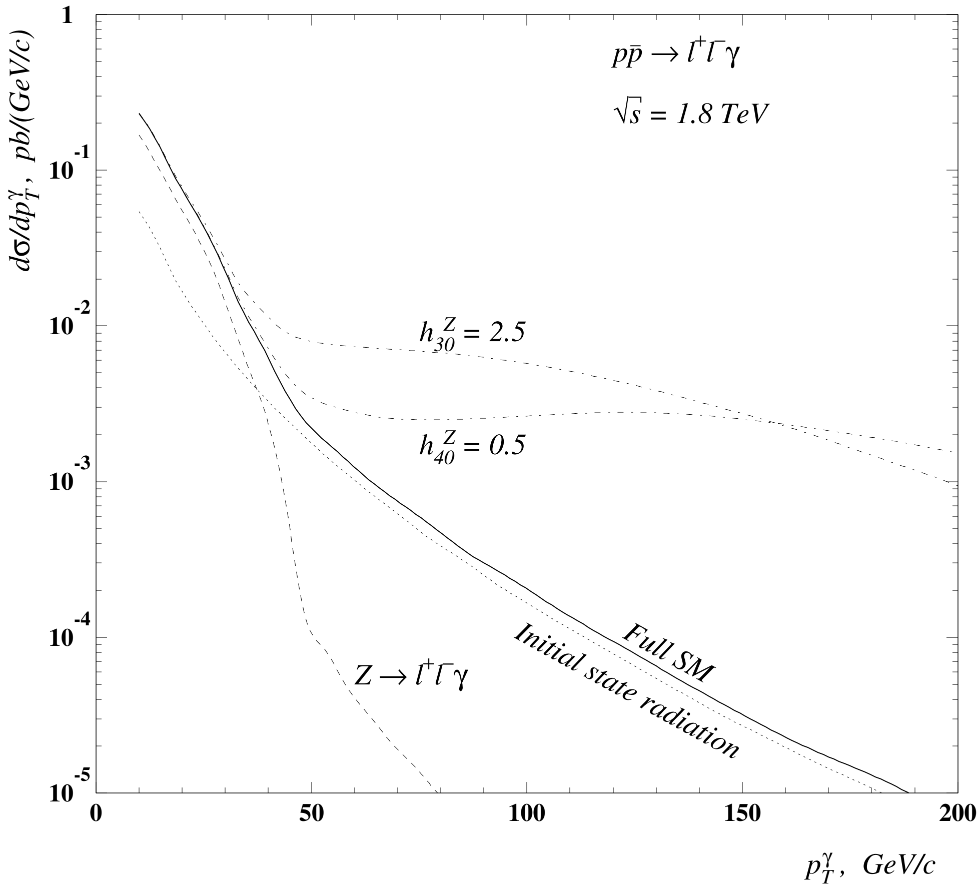

Figure 2.5: The p_T spectrum of the photon produced in the $p\bar{p} \to \ell^+\ell^-\gamma$ reaction for different processes contributing to this final state. For notations see text.

The most characteristic distribution for distinguishing between the SM and the anomalous coupling cases is the p_T^γ spectrum, as shown in Fig. 2.5. Anomalous couplings result in the emission of harder photons, and thus fitting the shape of the observed p_T^γ spectrum provides the tightest constraints on the anomalous couplings (see sec. 5.2). The $p_T^\gamma > 10$ GeV/c cut essentially does not affect the contributions from the anomalous couplings.

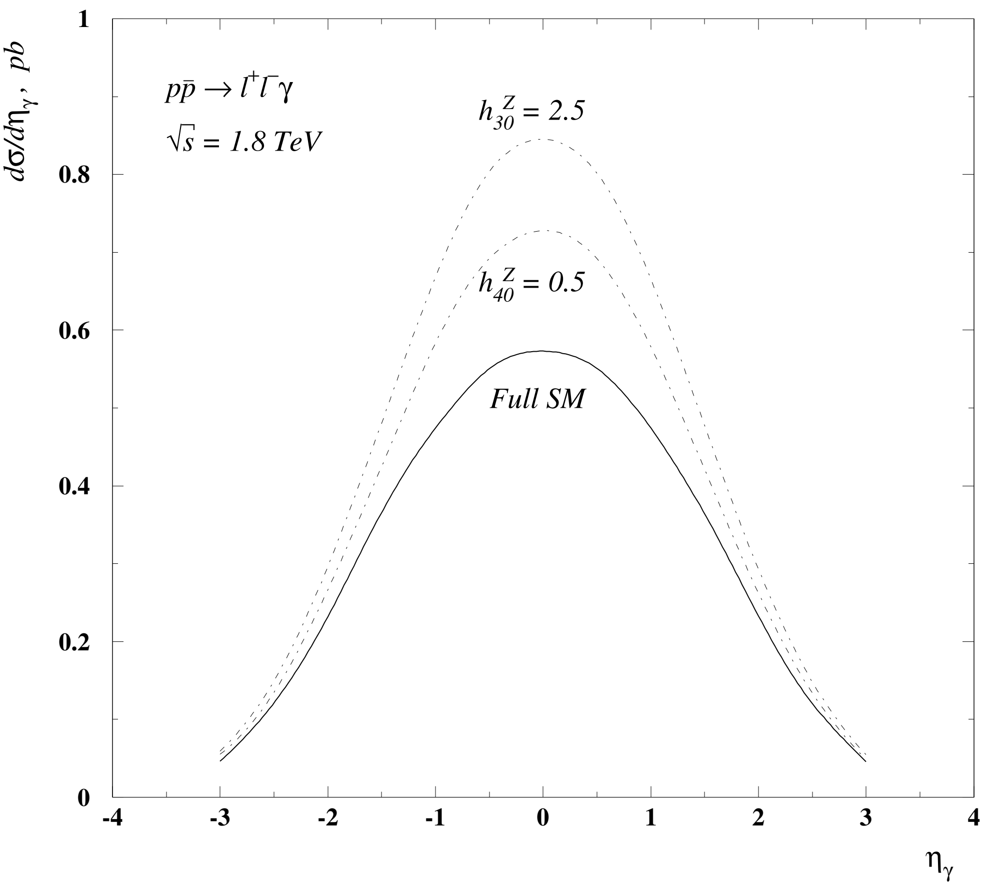

Figure 2.6: Pseudorapidity distribution for the photon produced in the $p\bar{p} \to \ell^+\ell^-\gamma$ reaction. For notations see text.

The photon pseudorapidity distribution is shown in Fig. 2.6. The contribution from the anomalous couplings is clearly concentrated in the central region. Both decay and initial state radiation contributions have the same bell shape, so they are not shown. A coverage of $|\eta_\gamma| < 2-3$ is thus quite sufficient to study the anomalous effects.

Finally, the separation distribution is shown in Fig. 2.7. Here we plot the ΔR between the photon and the closest lepton. As one would expect, the decay

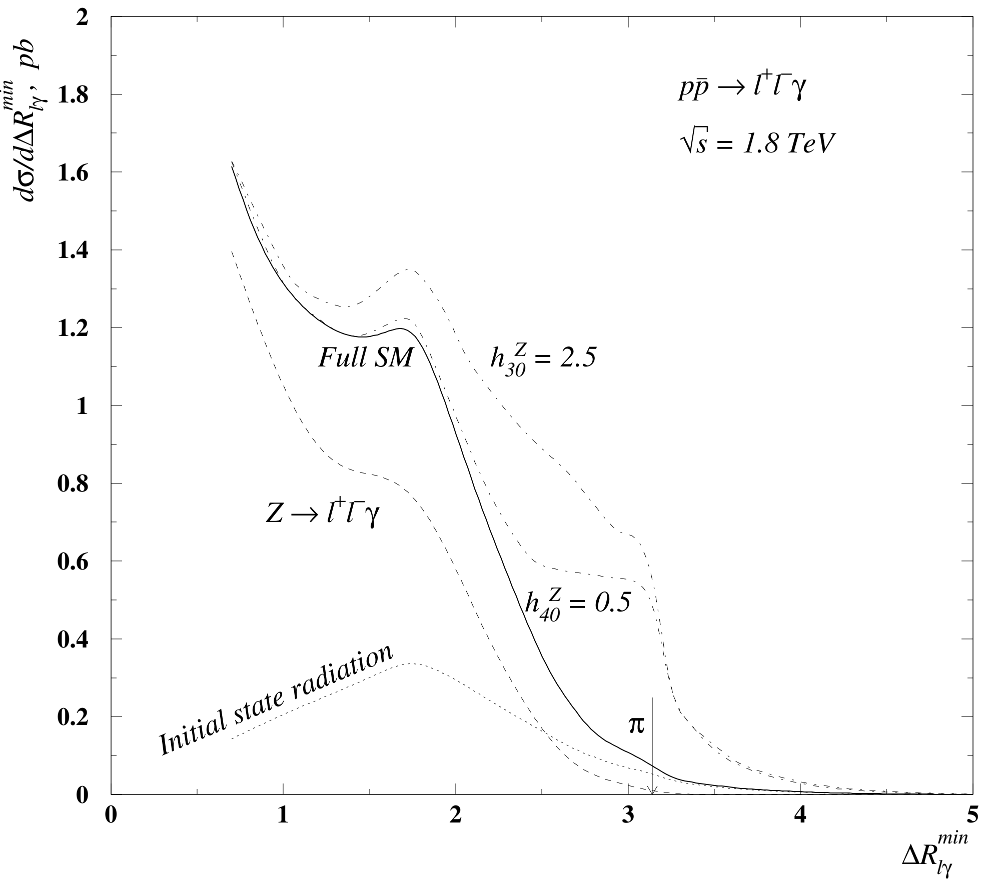

Figure 2.7: Minimum separation between the photon and charged leptons produced in the reaction (2.7) for different processes contributing to the $\ell^+\ell^-\gamma$ final state. For notations see text.

diagram contributions peak at low separations between one of the leptons and the photon, because of collinear nature of *bremsstrahlung*. The peak is not seen in the figure due to the ΔR-cut (2.8); instead there is a rapid decrease of the decay contributions as ΔR increases. Both initial state radiation and anomalous diagrams contribute for high lepton-photon separation. For the trilinear diagram (Fig. 2.2 (c)) the separation peaks approximately at π, which reflects the fact that the Z and the photon are very central and are emitted back-to-back with a very high transverse momentum which collapses both leptons of Z decay in the lab frame into a narrow cone around the parent Z momentum. The chosen cut $\Delta R \equiv \min(\Delta R_{\ell^+\gamma},\, \Delta R_{\ell^-\gamma}) > 0.7$ has essentially no effect on the anomalous coupling contribution.

Overall, there are significant differences between the differential cross sections of the reaction (2.7) in the SM and for anomalous couplings. Besides an increase of the total cross section for (2.7), photons produced by trilinear $ZV\gamma$ interactions have high transverse momenta, are central, and have a large separation from the leptons originating in the Z decay.

A potential background to the $p\bar{p} \rightarrow \ell^+\ell^-\gamma$ process originates from the $Z+j$ production with the jet hadronizing as a leading π^0. Such a jet might fake a photon in the detector due to the dominant $\pi^0 \rightarrow \gamma\gamma$ decay with two photon showers overlapping in the electromagnetic calorimeter. This background was estimated to be less than a few percent in [20] using the jet faking photon probability measured by the UA2 Collaboration [15] and a parton level Monte Carlo. A precise determination of this background for the DØ detector (using the real data) is discussed in sec. 4.5. This analysis confirms that the $Z+j$ background is small (of the order of few per cent) for DØ.

$p\overline{p} \rightarrow \nu\overline{\nu}\gamma$

In this section we will briefly describe the effects of the anomalous couplings in the other experimentally observable decay channel of the Z: $Z \rightarrow \nu\bar{\nu}$, which corresponds to a $\gamma\not{E}_T$ signature. Although $Z\gamma$ production in this decay channel has not yet been experimentally observed, it is interesting to explore the opportunities for studying anomalous couplings in the reaction

$$p\bar{p} \to \nu\bar{\nu}\gamma. \tag{2.9}$$

There are several very attractive features to this process. First, the decay diagrams (Fig. 2.2 (d,e)) vanish for the neutrino decay channel of the Z. Thus, the sensitivity to the anomalous couplings in reaction (2.9) should be higher than that in the process (2.7). Second, the observable anomalous cross section in the neutrino channel by itself is higher than that for the charged Z decay mode because $\mathrm{BR}(Z \to \nu\bar{\nu}) \approx 3 \cdot \mathrm{BR}(Z \to e^+e^- + \mu^+\mu^-)$ [9], and because the "acceptance" for neutrinos is not restricted by the detector geometry.

For the $Z \to \nu\bar{\nu}$ decay channel the basic set of cuts can be very simple:

$$p_T^\gamma > 10 \text{ GeV}/c, \;\; \not{E}_T \; > 10 \text{ GeV}, \;\; |\eta_\gamma| < 3.0. \tag{2.10}$$

At the Monte Carlo level, the $\not{E}_T$ requirement is satisfied automatically because of the transverse energy conservation. Experimentally, however, one needs an explicit $\not{E}_T$ cut because of the p_T-kick of the $Z\gamma$ system due to associated jet production.

The only observables in reaction (2.9) are the transverse momentum and the pseudorapidity of the photon. Contributions from the anomalous couplings are concentrated in the central region, as was the case for the charged lepton decay mode of the Z. Therefore the most interesting distribution is again the p_T^γ spectrum, as shown in Fig. 2.8 for the SM case and for the case of two different anomalous couplings: $h_{30}^Z = 2.5$ and $h_{40}^Z = 0.5$. The effect of the

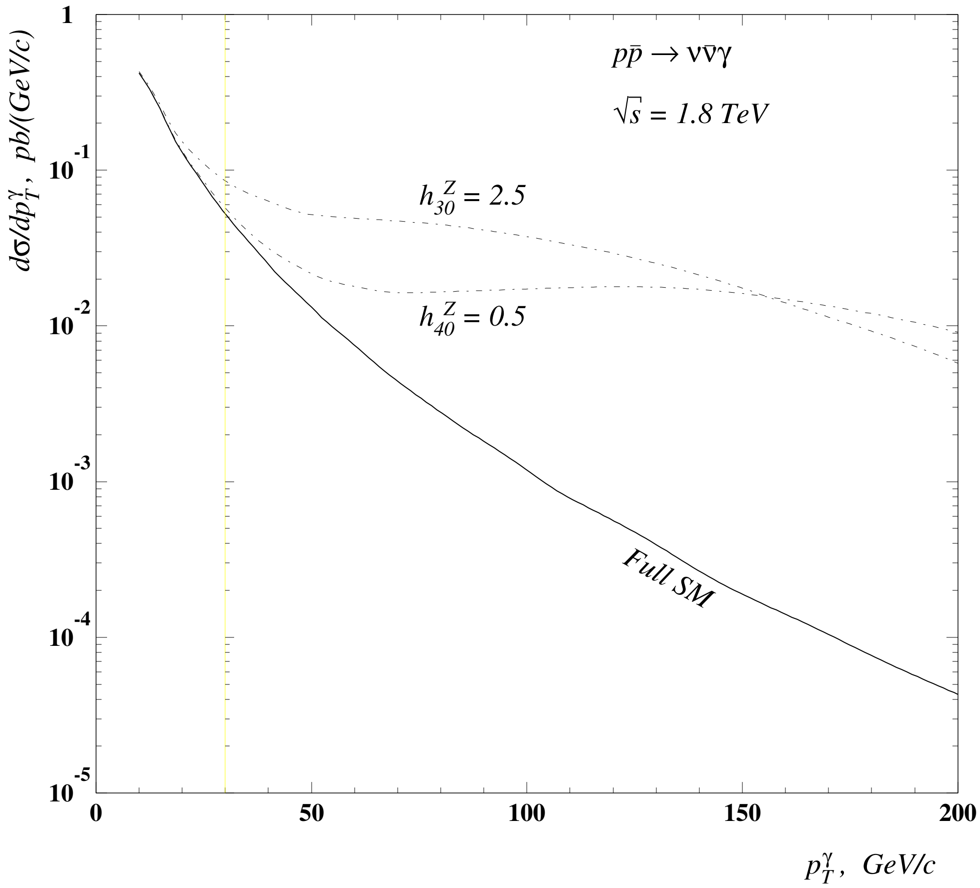

Figure 2.8: The p_T spectrum of the photon produced in the $p\bar{p} \to \nu\bar{\nu}\gamma$ reaction for the SM and anomalous coupling cases. For notations see text.

anomalous couplings is similar to that for the $\ell^+\ell^-\gamma$ final state. Quantitatively, however, it is stronger than for the charged decay mode of the Z, as one would expect. The theoretical cross sections for the SM and the anomalous cases for the set of cuts (2.10) for all three neutrino channels are as follows: $\sigma(SM) = 4.15$ pb, $\sigma(h^Z_{30} = 2.5) = 9.44$ pb, $\sigma(h^Z_{40} = 0.5) = 6.87$ pb. The anomalous and the SM cross sections differ by a factor of 2, which is to be compared with an increase of about 30% for the $Z \to \ell^+\ell^-$ decay mode.

The price for these advantages in the $\nu\bar{\nu}\gamma$ channel is two additional QCD background sources. The first one is dijet production with one jet faking the photon, whereas the second one fakes $\not{E}_T$ by escaping the detector through the beam-pipe, but still carrying away a significant amount of transverse energy. The probability for such a double-fake is, of course, very small, but the cross section for dijet production is several orders of magnitude higher than that for the reaction (2.9), so the background still might be significant. The other background is from direct photon $(j\gamma)$ production with the jet faking $\not{E}_T$ by the same mechanism. These two backgrounds are very detector-dependent, and a detailed study for the DØ detector has yet to be done. In addition, there is another very serious instrumental background for this detector due to the $q\bar{q} \to W \to e\bar{\nu}$ production with electron being misidentified as a photon due to the tracking detector inefficiency. This background will be discussed in sec. 4.4. However, simplified calculations of [20] show that both QCD backgrounds are small for $p_T^\gamma > 30$ GeV/c. Such a high p_T cut essentially does not affect the sensitivity to the anomalous couplings, as is clear from Fig. 2.8. The dotted Y-axis in this figure emphasizes the part of the spectrum above this p_T-cut.

2.3.4 Radiative and QCD Corrections

So far we have not discussed how the radiative and QCD corrections to the tree level diagrams (Fig. 2.2) change the signature for the anomalous couplings.

Radiative QED correction calculations at the one loop level ($\mathcal{O}(\alpha)$) for the $ZV\gamma$ vertices can be found in the literature (e.g. [30, 31]). They contribute only

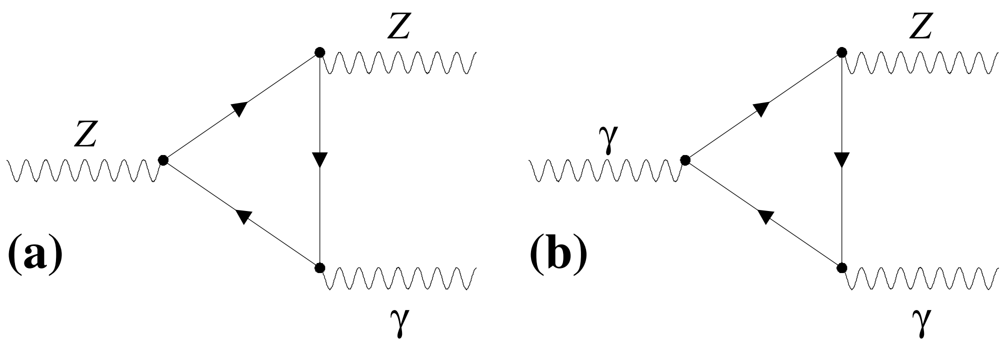

Figure 2.9: Typical loop correction diagrams for the (a) $ZZ\gamma$ and (b) $Z\gamma\gamma$ vertices.

to the CP-conserving couplings h_3^V, h_4^V. Typical triangle diagrams for these corrections are shown in Fig. 2.9. The triangular loops should be summed over the standard set of fermions [31]. The scale of these corrections is much less than the sensitivity of current and imaginable future experiments. For instance, for h_3^Z one finds [20]:

$$2.2 \cdot 10^{-4} < h_3^Z < 2.5 \cdot 10^{-4}$$

for top quark masses between 100 GeV/c^2 and 200 GeV/c^2. Thus, the QED radiative corrections can safely be neglected.

The QCD corrections, however, are important at Tevatron energies. Recently, some of these corrections were calculated to the NLL order for the SM case in the zero Z-width approximation [32]. There are two different types of processes which contribute to the set of diagrams in Fig. 2.2 at that level: virtual corrections and soft gluon emission. Typical Feynman diagrams for these corrections are shown in Fig. 2.10. Both types of the processes are of $\mathcal{O}(\alpha_s)$.

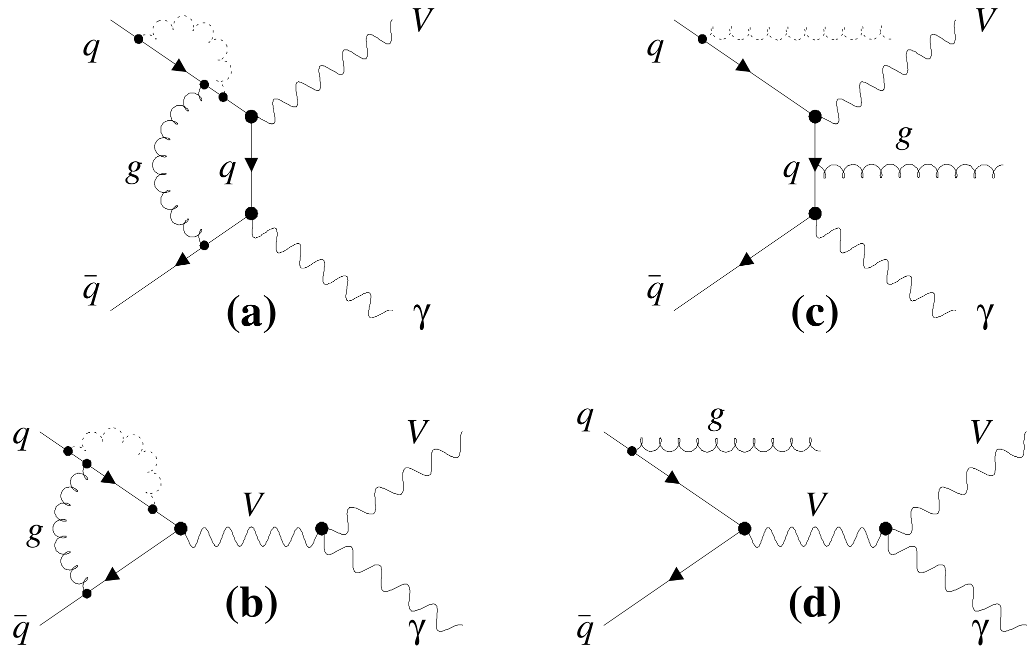

Figure 2.10: Virtual (a,b) and soft gluon radiation (c,d) QCD corrections to the initial state radiation (a,c) and trilinear (b,d) diagrams. Dotted lines show another possible type of gluon emission.

At present, the NLL QCD corrections are available only for the initial state radiation diagrams (see Fig. 2.10 (a,c)). As was shown in [32], the effect of these corrections is mostly a scaling of all discussed distributions by a constant factor. The contribution of $\mathcal{O}(\alpha_s)$ terms to the cross section depends on the set of cuts and is typically about 20% to 40%. These results justify using the so-called k-factor:

$$k = 1 + \frac{8\pi}{9}\alpha_s \approx 1.34$$

to scale the results of the LO calculations on which the Baur-Berger Monte Carlo [20] is based (see sec. 2.3.3 and 3.7).

The recent success of the same authors in calculating the NLL corrections for the anomalous $WW\gamma$ couplings [33] further shows that such a choice for the k-factor is a rather good approximation at Tevatron energies. At the LHC, however, a constant scaling will not work well because there is a significant p_T^γ dependence of the QCD corrections. Thus, the complete NLL calculation must be used for studying anomalous couplings at future higher energy hadron colliders.

Taking into account the QCD corrections is important in searches for anomalous couplings because, like the anomalous couplings themselves, they increase the cross section for the reactions (2.7) and (2.9). (At LHC and higher energies, the QCD corrections also change the shape of p_T^γ spectrum in a way similar to that of the anomalous couplings.)

2.4 Probing $ZZ\gamma$ and $Z\gamma\gamma$ Vertices in Low Energy Experiments

In this section we briefly describe the current limits on the anomalous couplings from low energy experiments. These experiments are sensitive to the anomalous trilinear couplings due to various loop corrections via penguin diagrams (see Fig. 2.11). Unlike the direct tests of couplings in high energy experiments, results at low energies are very sensitive to the regularization scheme and loop cutoff parameter used in the calculations, which makes them rather controversial and model dependent (e.g. [34]).

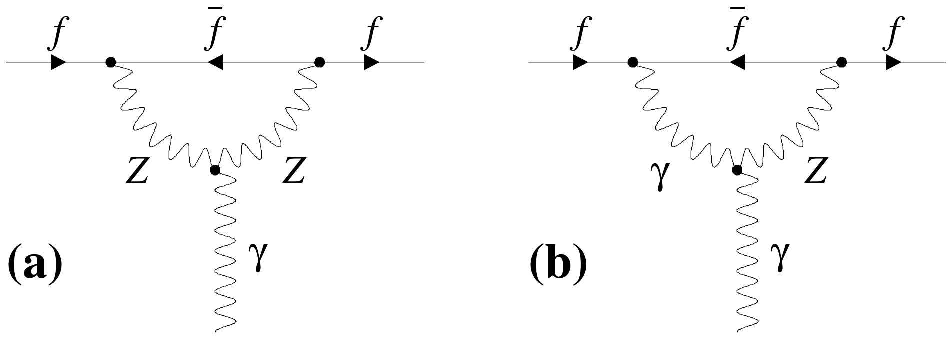

Figure 2.11: Typical loop correction diagrams contributing to the electromagnetic moments of a lepton or quark: a) via $ZZ\gamma$ vertex, b) via $Z\gamma\gamma$ vertex.

Generally, the limits from the loop-diagram corrections can be expressed in the following way [35]:

$$\left| h_{1,3}^V \cdot \left(\log \frac{\Lambda_c^2}{m_Z^2} + a \right) + h_{2,4}^V \cdot b \right| < C. \tag{2.11}$$

Here Λ_c is a cutoff parameter of the loop integration and a, $b = \mathcal{O}(1)$ are parameters depending on the regularization scheme used in the calculations.

It is important to stress that the limits on the anomalous couplings from (2.11) in the $(h_{1,3}^V,\, h_{2,4}^V)$ plane have the shape of a band, i.e. when both couplings are allowed to vary at the same time, the limits go to infinity, even if C is very small. Direct production experiments, on the contrary, produce closed contour limits in the same plane because the total cross section is a bilinear form of any pair of couplings (see sec. 2.3.3 and Chapter 5). However, when only one coupling is varied while the other is held fixed, the limits (2.11) can be very stringent.

The least model-dependent limits on CP-conserving couplings can be extracted from the recent CERN measurement of the gyromagnetic ratio for the muon (the so-called $(g-2)_\mu$ experiment) [36]. Various loop corrections to the magnetic moment of the muon are discussed in [37, 38]. The contributions from the $ZV\gamma$ anomalous couplings to the static electromagnetic properties of a fermion are shown in Fig. 2.11. Only the diagram Fig. 2.11 (b), however, contributes to the gyromagnetic ratio of the muon [38], thus making it sensitive only to the $Z\gamma\gamma$ CP-conserving couplings h_3^γ, h_4^γ. For instance, for $h_4^\gamma = 0$ one obtains at the 95% confidence level (CL) [20]:

$$\left| h_3^\gamma \log\left(\frac{\Lambda^2}{m_Z^2}\right)\right| < 9.$$

The most stringent constraints on the CP-violating couplings are expected from a precise measurement of the neutron electric dipole moment (EDM): $|d_n| < 1.2 \cdot 10^{-25}\ e \cdot \mathrm{cm}$ [39]. The formalism is similar to that discussed above for the $(g-2)_\mu$ limits, except that the CP-violating couplings contribute to the EDM. The limits on the anomalous $WW\gamma$ couplings from this experiment, calculated in [40], are of the order of 10^{-4} for both dimension six and dimension eight couplings. The limits on the anomalous $ZV\gamma$ couplings have not been calculated yet, but the expected accuracy is of the same order of magnitude: $|h_{1,2}^V| < \mathcal{O}(10^{-4})$ when only one coupling is allowed to vary at a time [28].

Another way of probing anomalous $ZV\gamma$ couplings is to search for radiative Z-decays at LEP and SLC. Since the $Z \to \gamma\gamma$ decay is prohibited by Yang's theorem [21], the only decays sensitive to the anomalous couplings are $Z \to \ell^+\ell^-\gamma$ and $Z \to \nu\bar{\nu}\gamma$. This is a direct and model-independent way to probe anomalous couplings at low energies. However, from Fig. 2.3 it is clear that the contribution of the anomalous couplings to the cross section at the

Z peak is very small (of the order of 1%). So, despite the very high sensitivity of the LEP experiments, the limits are not very tight. For instance, the measurement [41]: $BR(Z \to e^+e^-\gamma) < 5.2 \cdot 10^{-4}$, translates into the following 95% CL limits on the h_{i0}^V with the assumption of only one coupling varying at a time (form factor scale $\Lambda = 500$ GeV) [20]:

$$|h_{10,30}^Z| < 23, \quad |h_{20,40}^Z| < 62, \quad |h_{10,30}^\gamma| < 14, \quad |h_{20,40}^\gamma| < 99.$$

These limits are far beyond the unitarity limits given by equation (2.6). However, they can be significantly improved by fitting the transverse energy spectrum of the photon produced in association with the Z [6].

The sensitivity of the $Z \to \nu\bar{\nu}\gamma$ decays to the anomalous couplings is higher, but only $ZZ\gamma$ couplings can be measured in this channel because photons do not interact with neutrinos (the same reason why the decay diagrams for the reaction (2.9) vanish). The most recent preliminary results from LEP [6] based on the measurement [42] and the p_T^γ spectrum fit are as follows:

$$|h_{10,30}^Z| < 1.1, \quad |h_{20,40}^Z| < 3.1,$$

at 95% CL for the same form factor scale $\Lambda = 500$ GeV. The limits on $h_{20,40}^Z$ violate unitarity. A comparison of these preliminary results with the DØ and CDF data is discussed in Chapter 6.

Overall, the indirect limits on the anomalous $ZV\gamma$ couplings are at present significantly worse than those obtained in direct measurements, such as study of the radiative Z-decays at LEP or high-energy production of the $Z\gamma$ system in $p\bar{p}$ collisions at the Tevatron (see Chapters 5 and 6).

2.5 Models of the Anomalous Couplings

Do not expect too much of the end of the world.

Stanislaw J. Lec, "Aforyzmy. Fraszki"

Up to this point we have described the phenomenology of anomalous $ZV\gamma$ couplings without discussing any of the theoretical models which predict such phenomena. It should be stressed that there is no way to introduce a contact triple-boson interaction in any reasonable theory of anomalous couplings because of the high dimension of the operators in the vertex functions (2.3), (2.4). Any attempt to build a pointlike coupling with operators of dimension six and higher will result in a non-renormalizable theory. Thus the "blob" in Fig. 2.1 for the trilinear vertex is essential — it "hides" the exact structure of the non-pointlike interaction.

One possible way to introduce such a triple-boson interaction is through the triangle loop diagrams shown in Fig. 2.9. As it was discussed in sec. 2.3.4, the contribution of the regular SM QED-type of corrections is extremely small. However, it is possible to explain much stronger anomalous couplings by considering new types of particles in the triangular loops.

The most developed theory which gives rise to the CP-conserving anomalous couplings is the Minimal Supersymmetric Standard Model (MSSM) [43]. In this theory each particle has a supersymmetric (SUSY) partner. The partners for the fermions are bosons and *vice versa*. The MSSM also predicts an additional charged Higgs doublet in the gauge sector of the SM.

Although the SUSY partners have not yet been discovered, and masses below a hundred GeV have been excluded for most of them by various experiments [9], heavy supersymmetric particles may still contribute significantly to the anomalous couplings via the triangular loop diagrams.

These corrections were calculated for $WW\gamma$, WWZ couplings in several theoretical papers (see [44] and the references therein). Actual calculations of the loop corrections for the $ZV\gamma$ vertices have not been carried out yet. It is reasonable to expect that most of the corrections result in the anomalous couplings $h_i^V = \mathcal{O}(10^{-2})$ [28, 35]. But for certain values of the SUSY symmetry breaking parameters the deviations from the Standard Model can be much larger, and the dimension six CP-conserving couplings can be of order of 1. However, the application of perturbation theory in this region of parameter space is questionable. See [44] for details.

Currently, the only plausible model which predicts CP-violating $ZV\gamma$ couplings due to loop corrections is an extension of MSSM with two Higgs doublets [45]. The formalism of these calculations is given in Ref. [46].

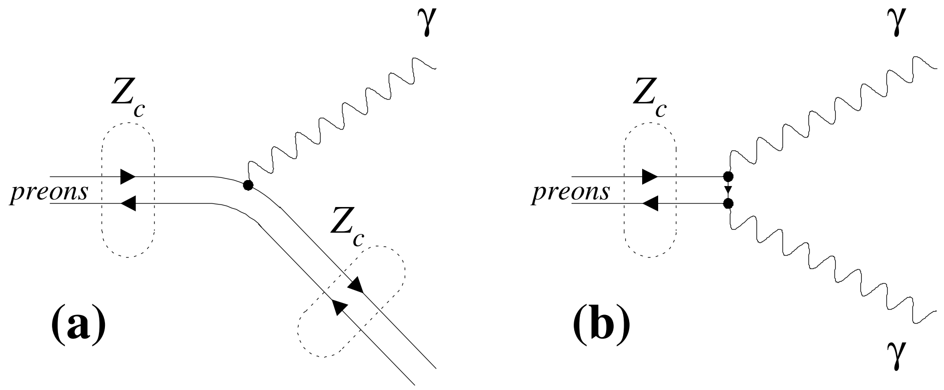

Figure 2.12: Trilinear gauge boson couplings in the models with a composite Z made of a preon-antipreon pair (Z_c): a) $ZZ\gamma$ vertex; b) $Z\gamma\gamma$ vertex.

Another theory of the anomalous $ZV\gamma$ couplings is one based on the assumption of a composite Z boson. In these models (e.g. [47]) the Z boson consists of a pair of hypothetical particles, a *preon* and an *antipreon*. The anomalous $ZV\gamma$ couplings in these theories naturally arise due to the diagrams in Fig. 2.12, analogous to the radiative meson decay diagrams [48]. The composite Z boson models predict anomalous couplings to be of the order of $h_i^V = 0.1 - 1$ [35].

The sensitivity of current experiments is not yet enough to rule out the MSSM or the models with a composite Z based on the limits on the anomalous couplings. This is a goal for future experiments (see Chapter 6).